SAND2019-1739C

Experimentally Enhanced Computations: Full-field validation of anisotropic yield functions for an aluminum 7079 extrusion

Sharlotte Kramer[1], Amanda Jones[1], Edmundo Corona[2] and Elizabeth Jones[3]

Sandia National Laboratories

[1] Experimental Environment Simulation Department

[2] Solid Mechanics Department

[3] Diagnostic Science and Engineering Department

1515 Eubank SE, Albuquerque, NM 87123

Keywords: Model Calibration; Computational Modeling; Anisotropy; Digital Image Correlation; Aluminum

This extended abstract summarizes the third in a three-part series of presentations (the first two presented at the last annual conference) addressing the calibration and validation of anisotropic yield functions in computational mechanics models for metals using full-field experimental data from Digital Image Correlation (DIC). In the first part, a calibration approach was employed using a simple tensile specimen geometry (homogeneous state of stress) manufactured in 12 orientations within an extruded cylinder of Al 7079. Several models that varied in their ability to capture anisotropic behavior were then calibrated using this tensile data. The investigated models, J_2 (isotropic), Hill-1948 (6 anisotropy parameters) and Barlat-Yld 2004-18p (18 anisotropy parameters) and their calibrations were validated using two specimen geometries in the second part. The first geometry was a double notch tension specimen, and the second one was a modified Brazilian disk compression specimen. The strengths and weaknesses of these specimen geometries, with respect to the measurable differences in mechanical response as a function of material orientation, were identified and motivated the next specimen validation geometry, which is the subject of this third part of our work.

Here, we present model validation results for a new specimen design. It consists of a wide tensile bar with a blind round hole at the center, as seen in Figure 1, subjected to tension along its long dimension. The idea behind the design is to introduce stress field inhomogeneity via the hole while still having a surface without cutouts on which deformation measurements with DIC are made. Specimens were manufactured in 4 orientations as shown in Figure 2. Specimens A, B and C had their long dimension along the axis of the cylindrical extrusion, while specimen D was aligned in the circumferential direction. The widths of specimens A and B were aligned in the radial and circumferential directions, respectively, while specimen C was oriented at 45^o to the radial direction. Specimen D had its width along the axis of the extrusion.

Figure 3 shows the continuous surface of one of the C specimens in the left column. In these figures, the x axis was taken as positive to the right while the y axis was positive upwards. The measured Hencky in-plane strain components ε_{xx}, ε_{yy} and ε_{xy} measured when the axial displacement was 0.0175 inches (1.4% of the length of the test section) are shown in Figures 3 (a), (c) and (e) respectively. The heterogeneous strain fields arise from the influence of the partial through hole on the opposite side, and the asymmetry in the fields is a convolution of the anisotropic material response and non-ideal boundary conditions. The right column in Figure 3 shows the predictions of the strain component fields obtained from finite element simulations of the experiment. Here, the model employed the Barlat-Yld 2004-18p yield function. The results are shown so the model is in the same orientation as in the experimental images. The results in Figure 3(b) are to be compared to those in 3 (a), those in 3 (d) to 3 (c) and those in 3(f) to 3 (e). Equal ranges and a similar, but not identical, color scheme has been chosen to represent the value of the strain components in the predictions as in the experiments. The simulation results reproduced the trends seen experimentally reasonably well. In particular, note that the patterns for both ε_{xx} and ε_{yy} are shifted to the right. In the case of

ε_{xy} the asymmetry of the pattern seen experimentally is also captured well by the analysis. Each specimen orientation exhibited its own unique strain patterns, and in all cases the simulation results were in good agreement, similar to what was presented here.

In the course of the work, it was noted that the ideal boundary conditions used in the analysis, in which the lower edge of the model was pulled straight down while the top edge was kept fixed, matched the *overall* motion of the measured boundary displacements. However, small off-axis rotations and displacements were observed in the experiments. These non-ideal boundary conditions contributed to the asymmetry observed in the experimental strain fields. Accounting for such second-order effects, as well as processing the predicted displacement fields through the same software as the DIC measurements, will likely improve the comparison between experiments and simulations.

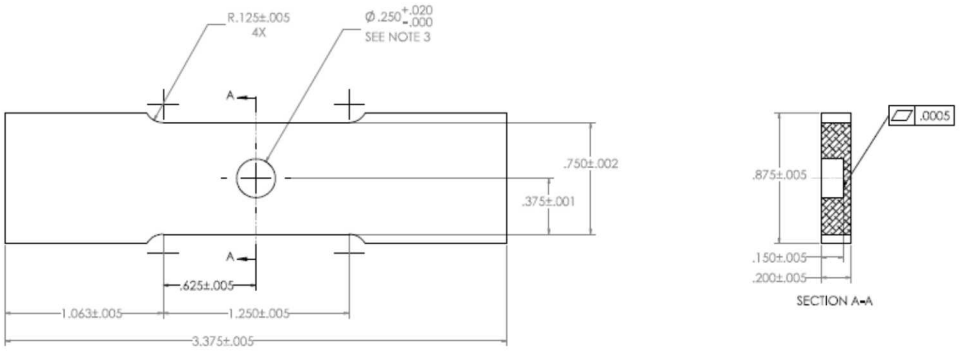

Figure 1: Schematic and dimensions of the blind hole specimens.

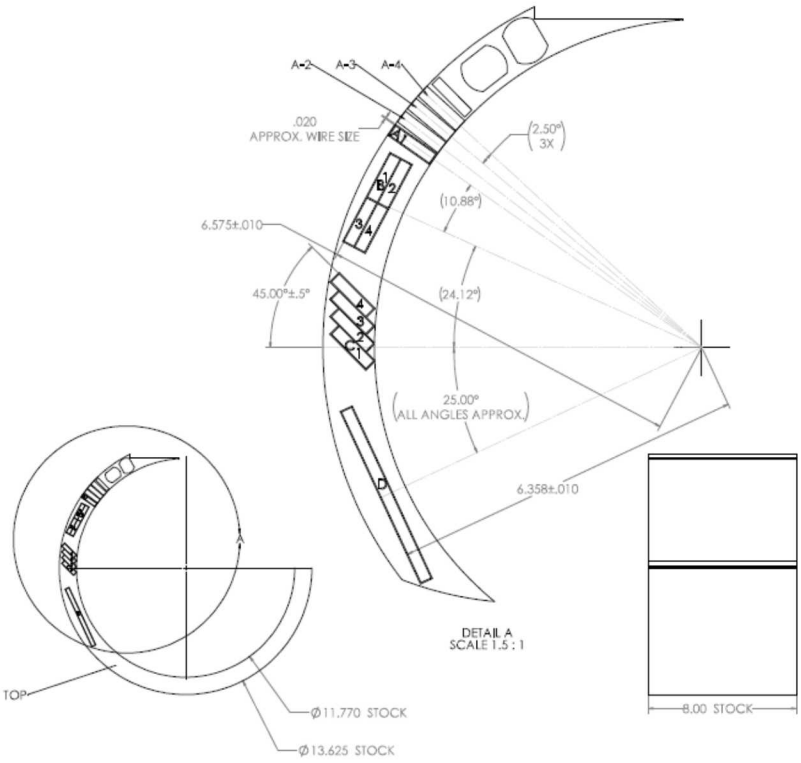

Figure 2: Schematic showing how the specimens were extracted in four different directions with respect to the extrusion.

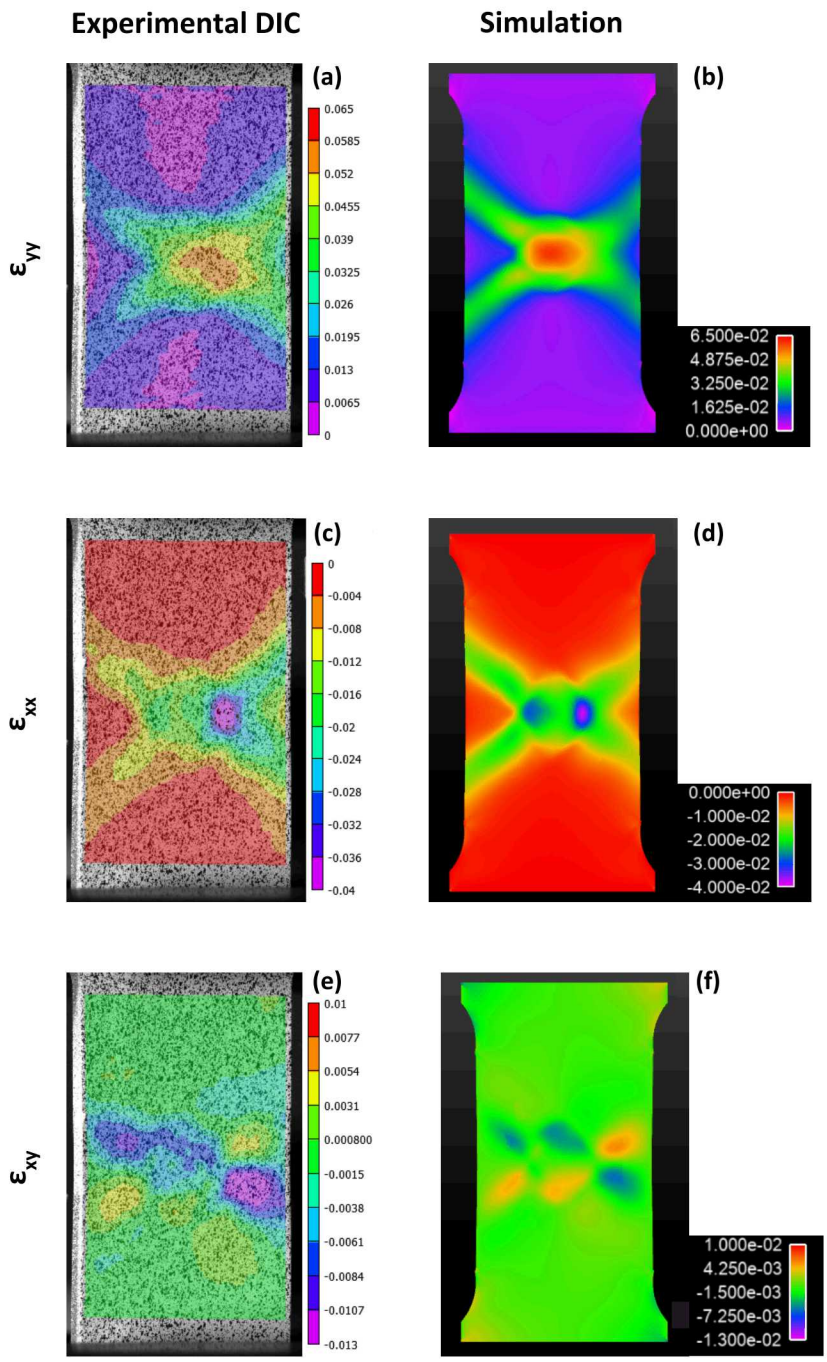

Figure 3: DIC Hencky ε_{xx}, $\varepsilon_{yy,\text{ and }}\varepsilon_{xy}$ strain fields (a,c,e) compared to simulation results (b,d,f) for the specimen cut at a 45 degree angle to the radial line (Specimen C).

ACKNOWLEDGEMENTS

Sandia National Laboratories is a multi-mission laboratory managed and operated by National Technology and Engineering Solutions of Sandia, LLC., a wholly owned subsidiary of Honeywell International, Inc., for the U.S. Department of Energy's National Nuclear Security Administration under contract DE-NA-0003525